



HAL
open science

Environment dependence of K_{Ic} of glass

T. To, Fabrice Célarié, Yann Gueguen, N.G. Brou, C. Lim, R. Horm, V. Burgaud, M.L. Fur, J. Chollet, H. Orain, et al.

► To cite this version:

T. To, Fabrice Célarié, Yann Gueguen, N.G. Brou, C. Lim, et al.. Environment dependence of K_{Ic} of glass. *Journal of Non-Crystalline Solids*, 2021, 566, pp.120873. 10.1016/j.jnoncrysol.2021.120873 . hal-03249478

HAL Id: hal-03249478

<https://hal.science/hal-03249478>

Submitted on 24 May 2023

HAL is a multi-disciplinary open access archive for the deposit and dissemination of scientific research documents, whether they are published or not. The documents may come from teaching and research institutions in France or abroad, or from public or private research centers.

L'archive ouverte pluridisciplinaire **HAL**, est destinée au dépôt et à la diffusion de documents scientifiques de niveau recherche, publiés ou non, émanant des établissements d'enseignement et de recherche français ou étrangers, des laboratoires publics ou privés.



Distributed under a Creative Commons Attribution - NonCommercial 4.0 International License

1 **Environment dependence of K_{Ic} of glass**

2 Theany To¹, Fabrice Célarié¹, Yann Gueguen¹, N'Goan Brou¹, Chhoung Lim¹, Rithymarady Horm¹, Vincent
3 Burgaud¹, Mickaël Le Fur¹, Julien Chollet¹, Hervé Orain¹, Tanguy Rouxel^{1,2*}

4 ¹ *Mechanics and Glass Department, Institut de Physique de Rennes, UMR 6251 URI-CNRS, Université de*
5 *Rennes 1, Campus de Beaulieu, 35042 Rennes Cedex, France*

6 ² *Institut Universitaire de France*

7 * Corresponding author. E-mail: tanguy.rouxel@univ-rennes1.fr

8

9 **Abstract**

10 **The** role of temperature (T) and moisture on fracture toughness (K_{Ic}) of glasses, as measured by the single-
11 edge precracked beam method (SEPB), **is investigated**. The brittle to ductile temperature, **shown** by an
12 increase of K_{Ic} , is $\sim T_g$. At T below $0.9T_g$, the decrease of the bond strength with T results in the decrease of
13 both the fracture surface energy and Young's modulus, so that K_{Ic} decreases with T . From above T_g to below
14 $1.1T_g$, the work of fracture increases because of dissipative processes, including confined viscoplasticity and
15 blunting at the crack front. From $1.1T_g$, viscous flow extends to the whole specimen and becomes more
16 uniform, resulting in the macroscopic deformation of the specimen, eventually preventing against fracture.
17 The results on humidity sensitive glasses show that both precracking and final fracture steps need to be
18 performed in inert environment to meet the intrinsic K_{Ic} value, unless the test is fast enough.

19 **Keywords:** Fracture toughness, single-edge precracked beam (SEPB), environment dependence, brittle to
20 ductile transition (BDT)

1 **1. Introduction**

2 Although the environment dependence of the fracture toughness (K_{Ic}) of glasses and ceramics is important
3 for their application in service conditions it is not well understood, and was scarcely reported. Most
4 publications focused on the effect of temperature for ceramics [1–8], and of humidity for **amorphous silica**
5 (**a-SiO₂**) and window glass [9–11].

6 **The SEPB test** is a reliable and self-consistent method, which is based on the generation of a sharp precrack,
7 with sharpness down to atomic scale [12–15]. However, due to inherent difficulties in specimen preparation
8 and testing conditions, **this** method has not been used in environmentally controlled **atmosphere** so far.

9 In this work, the SEPB method is applied to glasses samples up to $1.11T_g$, and results are compared to
10 previously published ones [10,11]. **Both the** precracking and **the** final fracture stages of the method are
11 performed in controlled atmosphere.

12 Regarding the temperature dependence, four glasses from silicate, borate and oxynitride chemical systems
13 were selected. As far as relatively small loading rates are applied (quasi-static regime), typically for $dK_I/dt \leq$
14 $10 \text{ MPa}\cdot\sqrt{\text{m}}\cdot\text{s}^{-1}$, which corresponds to strain-rates, $\dot{\epsilon}$, below 10^{-2} s^{-1} , the brittle to ductile transition
15 temperature is expected to be at around T_g . For the environment dependence, four commercial glasses
16 (silicate and borosilicate systems) were **investigated**. Cross-head speeds ranging from $0.01 \mu\text{m}\cdot\text{s}^{-1}$ and to 15
17 $\mu\text{m}\cdot\text{s}^{-1}$ were applied during the SEPB bending experiment to investigate the possible influence of the crack
18 velocity. Finally, results from previously published SEPB experiments in ambient atmosphere, where only
19 the final fracture stage was conducted in dry N₂ atmosphere [14,15], and present results (both precracking
20 and final fracture steps in dry argon atmosphere) are compared.

21 **2. Experimental Procedures**

22 The seven glass compositions that were used are given in Tables 1 and 2. Among these glasses four grades
23 covering a large T_g range, from 673 K to 1207 K, were used to study the effect of temperature on K_{Ic} (Table
24 1). Four silica-rich (70-100 mol.%) grades were used to investigate the effect of humidity (Table 2). The
25 density (ρ) was measured using $3 \times 4 \times 20 \text{ mm}^3$ specimens by means of Archimedes principle of buoyancy

1 in distilled water. The elastic moduli (Young's modulus, E and shear modulus, G) and Poisson's ratio (ν)
2 were determined by means of ultrasonic echography using 10 MHz piezoelectric transducers:

$$G = \rho V_T^2 \quad (1)$$

$$E = \rho \frac{3V_L^2 - 4V_T^2}{(V_L/V_T)^2 - 1} \quad (2)$$

$$\nu = \frac{E}{2G} - 1 \quad (3)$$

3 Where V_L and V_T are the longitudinal and transverse wave velocities respectively.

4

5 2.1. K_{Ic} at elevated temperatures

6 High temperature K_{Ic} measurements (SEPB method) were performed at $0.35T_g$, $0.93T_g$, T_g , $1.03T_g$, $1.05T_g$,
7 $1.07T_g$ and $1.11T_g$. In order to use the SEPB technique, parallelepiped bars were cut from glass batches using
8 a diamond saw to get $3 \times 4 \times 20$ mm³ bars, which were further polished down to 3 μ m diamond paste. A
9 series of 10 N Vickers indents, each distant by 200 μ m to the adjacent ones, were aligned at the center of the
10 3×20 mm² tensile face, along with broadness ($B = 3$ mm) as detailed in Ref. [15]. Specimens were then set
11 in a bridge-flexure anvil [16] allowing for a precrack to be generated, as long as about half of the specimen
12 width ($W = 4$ mm). During the bridge-flexure test, the indented specimen experiences a tensile stress at the
13 lower part (near the indented surface) and a compressive one at the upper part. In such a situation, the
14 precrack starts from the indents, grows and stops at around the center of the beam where it meets the
15 compressive field. The precracked specimens were finally fractured at elevated temperatures with an
16 aluminum oxide three-point bending device with a span length of 15 mm. A heating rate of 12 K·min⁻¹ was
17 used and a thermocouple was positioned close (~ 1 mm) to the center of the specimen. After cooling down to
18 room temperature, the precrack length was measured (fractography), and K_{Ic} was calculated from the
19 maximum load [15]. All experiments were conducted in ambient atmosphere (~ 60 %) with a cross-head
20 speed of 15 μ m·s⁻¹ (loading rate of about 10 MPa· \sqrt{m} ·s⁻¹), and the test temperature was known with an
21 accuracy better than ± 1 K.

22 2.2. K_{Ic} in dry argon gas atmosphere

1 Samples from the four glass grades in Table 2 were characterized both in dry argon gas ($T = 20\text{ }^{\circ}\text{C}$; RH ~ 0)
2 and in ambient atmosphere ($T = 20\text{ }^{\circ}\text{C}$; RH = 60 %). In the case of SEPB experiments conducted in dry
3 argon gas, both precrack and final fracture steps were performed in a glove box filled with high purity dry
4 argon. After indentation in ambient conditions (to ease the precrack formation), the bar specimens were
5 placed in the anvil for precracking inside a glove box (**Figure 1**) and loaded by means of a portable uniaxial
6 testing machine (Deben, UK). A camera focused on the middle of the specimen (where indentation was
7 performed) was used to follow in-situ the precracking stage and to observe the pop-in of the precrack. The
8 machine was manually stopped once the precrack appeared. The precracked specimen was then loaded in
9 three-point bending (span length of 15 mm) **set-up positioning in a homemade uniaxial machine**, and the load
10 was monitored by means of a 50 N capacity load cell (K25, Scaime Company, France) with an accuracy
11 better than 0.001 N. The broken specimens were then taken out of the argon gas box to measure the precrack
12 length and K_{Ic} was calculated from the maximum load and the measured precrack length (see **ref. [15] for**
13 **details**). In ambient conditions (RH = 60 %), it was previously shown that the results derived from unstable
14 tests (that is where the load-displacement curve exhibits some disruption or fast unloading once the
15 maximum load is passed) are free from environment incidence (no slow crack growth) as they are associated
16 to large crack velocities. Unstable test in ambient conditions were obtained at a cross-head speed between 5
17 and $15\text{ }\mu\text{m}\cdot\text{s}^{-1}$. The cross-head speed for the experiments in the glove box was set at $0.05\text{ }\mu\text{m}\cdot\text{s}^{-1}$, but for 1
18 extra experiment on a SLS specimen where a cross-head speed of $5\text{ }\mu\text{m}\cdot\text{s}^{-1}$ (100 times faster than for other
19 experiments) was chosen for comparison.

20

21 **3. Results**

22 **3.1. SEPB test evaluation**

23 **Among one hundred thirty five tests, nine were found invalid and were discarded because either (i) the**
24 **precrack was too short (less than 25% of the width, W in **Figure 2**) or too long (more than 75% of W), or (ii)**
25 **the precrack front was uneven between both sides of the broadness, B in **Figure 2** (more than 10% difference**
26 **between the average precrack length and any measurement at 25%, 50% and 75% of B , i.e. $|(a - a_1)/a| >$**
27 **0.10 as shown in **Figure 1**), or (iii) the angle between the precrack and the final fracture was larger than 10°**
28 **(**Figure 3**). These unsuitable conditions lead to over- or under-estimated values for K_{Ic} [14,15]. During the**

1 bridge-compression stage (**Figure 2a**), the precrack can be stable or unstable [15]. In our case, the precrack
2 is unstable and is referred to as a pop-in precrack, i.e. the precrack suddenly occurred just after the onset of
3 extension from the indents, as shown in **Figure 2**. **Figure 2b** shows the load-displacement curve during the
4 pop-in precrack formation which is observed in **Figures 2c** and **2d**. An example of post-fracturing
5 investigation is shown in **Figure 3**. The precrack length used in the K_{Ic} determination is measured from
6 **Figure 3a**, and the angle between the precrack and the final fracture is measured from **Figure 3b**. The
7 measured angles used in this Results section are between 0 and 4°.

8 3.2. Temperature dependence of K_{Ic}

9 The dependence of K_{Ic} on temperature is illustrated in **Figure 4** (data taken from **Table 2**). At high
10 temperature, viscous flow induces some energy dissipation at the vicinity of the crack front (confined
11 viscoplasticity) from T_g to $1.05 T_g$ and then at a larger scale at higher temperature, where viscoplastic flow
12 eventually extends through the overall thickness of the specimen depending on the loading rate, and
13 preventing against fracture. As a result of this energy dissipation, the experimental values for K_{Ic} are no
14 longer intrinsic in this temperature range. Recall that the intrinsic toughness is related to Young's modulus
15 and to the fracture surface energy (intrinsic), γ , following:

$$K_{Ic}^{\text{intrinsic}} = \sqrt{2\gamma E'} \quad (4)$$

16 where $E' = E$ in plane stress and $E' = E/(1-\nu^2)$ in plane strain. Since both E' and γ decrease upon heating
17 (consistently with the weakening of the interatomic bond strength), K_{Ic} is also expected to decrease. This is
18 actually what is observed from RT to $\sim 0.8T_g$. However, experimental investigation reported on glasses (as
19 well as on any material on approaching the brittle to ductile transition, if any) mostly show a rapid increase
20 of K_{Ic} above T_g [10,11,17], but for a-SiO₂ glass [9,10], which exhibits little de-structuration and a weak
21 decrease of the viscosity coefficient through the T_g range. This is because as temperature gets close to T_g the
22 characteristic relaxation time constant become comparable to the experimental time, which allows for
23 viscous stress relaxation to occur at the crack front. As a matter of fact, K_{Ic} becomes also loading-rate
24 dependent above $0.8T_g$. A transition temperature is observed above which crack tip blunting occurs: this is
25 the brittle-ductile transition (BDT) [11]. The loading rate dependence of the effective fracture toughness
26 ($K_{Ic}(T)/K_{Ic}(T_{RT})$) is illustrated in **Figure 4a** for SLS. With a loading rate of $2 \text{ MPa}\cdot\sqrt{\text{m}}\cdot\text{s}^{-1}$, the BDT of SLS

1 glass is at $\sim 0.89T_g$ and with a loading rate of $4 \text{ MPa}\cdot\sqrt{\text{m}}\cdot\text{s}^{-1}$, it is at $\sim 0.97T_g$ [11]. With the loading rates of 5
2 and $8 \text{ MPa}\cdot\sqrt{\text{m}}\cdot\text{s}^{-1}$, the BDT is at $\sim T_g$ [10,11]. With the loading rate of $10 \text{ MPa}\cdot\sqrt{\text{m}}\cdot\text{s}^{-1}$, the BDT of SLS is
3 $\sim 1.05T_g$. The temperature dependence on K_{Ic} for the four studied glasses at the rate of $4 \text{ MPa}\cdot\sqrt{\text{m}}\cdot\text{s}^{-1}$ is shown
4 in **Figure 4b**, together with additional results for SLS (window glass) and SiNaMgO at $10 \text{ MPa}\cdot\sqrt{\text{m}}\cdot\text{s}^{-1}$. The
5 BDT for all glasses at the rate of $4 \text{ MPa}\cdot\sqrt{\text{m}}\cdot\text{s}^{-1}$ are $\sim 0.8T_g$ for N-Glass and $0.9T_g$ for the other compositions.
6 At the rate of $10 \text{ MPa}\cdot\sqrt{\text{m}}\cdot\text{s}^{-1}$, the BDT is ~ 1.05 for both SLS and SiNaMgO.

7 *3.3.Environment dependence of K_{Ic} at room temperature*

8 The cross-head speed (CHS) dependence on K_{Ic} of SLS, a-SiO₂, Borofloat and BK7 is shown in Table 3. In
9 ambient conditions, K_{Ic} is found to depend much on the CHS. With a CHS of $0.5 \mu\text{m}\cdot\text{s}^{-1}$, the test is stable and
10 $K_{Ic} \sim 0.5 \text{ MPa}\cdot\sqrt{\text{m}}$ for all glass compositions. On the other hand, with a CHS of $5 \mu\text{m}\cdot\text{s}^{-1}$, the test is unstable
11 and K_{Ic} is as high as 0.70, 0.69, 0.65 and $0.82 \text{ MPa}\cdot\sqrt{\text{m}}$ for SLS, a-SiO₂, Borofloat and BK7, respectively. In
12 the case of the unstable test (the load reaches a maximum value and then drops sharply as the crack suddenly
13 extends) the crack velocity is fast enough to avoid moisture effects at the crack front, so that the
14 experimental K_{Ic} value is not affected by stress corrosion (region 3 of the crack velocity- K_I curve, after
15 Wiederhorn [18]) [15]. Besides, there is no rate dependence in the case of experiments performed in argon
16 atmosphere. In this latter case, values of K_{Ic} obtained with a CHS of $5 \mu\text{m}\cdot\text{s}^{-1}$ agree with those obtained at a
17 rate 100 times slower ($0.05 \mu\text{m}\cdot\text{s}^{-1}$). It is thus concluded that dry argon atmosphere prevents stress-corrosion
18 (also called static fatigue).

19 Values for K_{Ic} as measured by means of the SEPB method in different atmosphere or determined ab-initio by
20 means of a simple theoretical approach (after Ref. [12]) is shown in **Table 4**. For all gasses, values measured
21 in argon atmosphere are in agreement with those measured in ambient atmosphere using unstable tests (see
22 ref. [15] for details) and are remarkably close to the theoretical ones [12]. In contrast, the average values
23 measured in N₂ atmosphere are systematically a bit larger than the other values. This might result from the
24 use of the 4-point bending device (in [14]) instead of the 3-point bending one (in this study). Recall that
25 Quinn et al. [14] performed only the final fracture stage in dry N₂ while both precracking and final fracture
26 stages were performed in dry argon in the present work. The agreement between these independent series of
27 measurements suggests that the restricting environment controlled conditions solely to the final fracture stage

1 is enough to get rid of the stress corrosion effects. Besides, experiments can be done in ambient atmosphere
 2 providing the CHS is large enough to induce a crack velocity large enough to insure a fatigue-free behavior
 3 (region III of the Wiederhorn's v-K curve [18]).

4 **4. Discussion**

5 *4.1. Temperature dependence of K_{Ic}*

6 The fracture behavior of glass at elevated temperatures exhibits three regimes: elastic and brittle from RT to
 7 $0.9 T_g$, semi-ductile with some local viscoelasticity in the T_g range, and viscoplastic (ductile) above $1.1 T_g$ as
 8 illustrated in **Figure 2** and corroborated by the absence of breakage in **Table 3** above $1.1 T_g$. Considering for
 9 example the loading rate of $4 \text{ MPa}\cdot\sqrt{\text{m}}\cdot\text{s}^{-1}$, regions I (Brittle), II (BDT) and III (Ductile) are associated with
 10 temperatures from RT to $0.8T_g$, $0.8T_g$ to $0.93T_g$ and $0.93T_g$ to above, respectively.

11 In region I and II, K_{Ic} decreases as the temperature is increased (**Figure 2**). This is because the bond strength
 12 and thus both E and γ decrease on heating, and so does K_{Ic} (Eq. 2). The temperature dependence of the elastic
 13 moduli of glasses from different chemical systems was previously reported [10,19–22]. In most cases but for
 14 amorphous silica ($\alpha\text{-SiO}_2$) E decreases on heating. In the case of $\alpha\text{-SiO}_2$ (considered as an anomalous glass),
 15 a slight increase of E is observed below T_g and a light increase of K_{Ic} follows [9,10]. Nevertheless, for both
 16 normal and anomalous glasses, the fracture surface energy is expected to decrease as temperature is
 17 increased because of the weakening of the atomic bonding along the crack path. The decrease of the fracture
 18 surface energy (γ^{loss}) is defined as:

$$\gamma^{\text{loss}} = \gamma - \gamma^T. \quad (5)$$

19 where γ is the surface energy at room temperature and γ^T the one at elevated temperature.

20 In the BDT region (II), taking E and ν from Refs. [19,23], γ^{loss} of $0.48 \text{ J}\cdot\text{m}^{-2}$, $0.93 \text{ J}\cdot\text{m}^{-2}$ and $0.34 \text{ J}\cdot\text{m}^{-2}$ for SLS,
 21 N-Glass, and BPbCuO were calculated, respectively. A simple theoretical model [12] led to the following
 22 expression for γ :

$$\gamma = \frac{1}{2} \left(\frac{\rho}{M_0} \right)^{2/3} N^{-1/3} \sum_i x_i n_i U_{0i}, \quad (6)$$

1 where M_0 is the molar mass, N is the Avogadro number, x_i the stoichiometric fraction of the species involved
2 in the i^{th} bonding energy U_{0i} . By neglecting the variation of ρ (with a large possible thermal expansion
3 coefficient (of flat SLS glass) of $9.5 \times 10^{-6} \text{ K}^{-1}$, the volume change $\Delta\rho = 2.2\% \rho$ at $1.1T_g$), $\gamma/\gamma^T =$
4 $(\sum_i x_i n_i U_{0i}) / (\sum_i x_i n_i U_{0i})^T = 1.20, 1.24$ and 1.21 for SLS, N-Glass, and BPbCuO, respectively. Therefore, for
5 the three glasses of concern, the mean bonding energy along the fracture path is about 83 % of its value at
6 room temperature at the BDT. The same conclusion is met for a loading rate of $10 \text{ MPa} \cdot \sqrt{\text{m}} \cdot \text{s}^{-1}$. Furthermore,
7 when the actual values of E and ν at elevated temperature are used together with γ^T at the BDT temperature,
8 the predicted value for K_{Ic} (Eq. 4) is in agreement with the experimental one.

9 In region III, the apparent toughness increases sharply from a value below K_{Ic} (RT) to over 1.5 times the
10 initial value. In this range, fracture is eventually avoided due to viscoplastic relaxation, as seen in **Figure 5**.
11 On the one hand, the crack tip becomes blunted (**Figure 5b**), which requires larger load to propagate the
12 crack. On the other hand, from $1.1T_g$, the glass behaves in a more and more viscoplastic manner so that most
13 of the mechanical energy is dissipated in the flow process. It is suggested that the load peaks for
14 displacements of 0.15 and 0.4 mm correspond to onsets of crack extension steps but the load ultimately reach
15 a slowly increasing plateau, which corresponds to the viscous flow. Indeed, a load between 15 and 20 N is
16 associated with a stress (σ) of about 10 MPa, and the imposed strain-rate ($\dot{\epsilon}$), derived from the displacement
17 rate ($5 \mu\text{m} \cdot \text{s}^{-1}$ for a $4 \text{ MPa} \cdot \sqrt{\text{m}} \cdot \text{s}^{-1}$ loading rate), is about $0.5 \times 10^{-3} \cdot \text{s}^{-1}$. This results in a viscosity coefficient,
18 $\eta = \sigma / (3\dot{\epsilon})$ of about $0.7 \times 10^{10} \text{ Pa} \cdot \text{s}$, which is in agreement with the glass viscosity at $1.1T_g$. It is noteworthy
19 that, for most glasses ν reaches values larger than 0.3 above $1.1T_g$, which also corroborates the occurrence
20 of ductility as was recently discussed elsewhere [24].

21 *4.1.1. Pre-crack tip analysis*

22 The crack front geometrical and physical characteristics are fundamental to understand the changes of the
23 apparent toughness. For example, a diffuse damage zone at the vicinity of the tip was observed to give birth
24 to relatively large apparent toughness values for metallic glasses, thanks to energy dissipation [25]. In such
25 glasses, shear bands may occur and accommodate the singular tip stress field, especially in the case of
26 glasses with large Poisson's ratio (over 0,33), where sliding predominates over volume change [26]. The

1 high Poisson's ratio together with high nanoductility has been shown on glasses with relatively low
2 covalency interatomic bonding character and high structural disorder [27]. However, the present glasses lie
3 at the opposite side, with low Poisson's ratio and high covalency (directional) bonds [28]. Consequently, no
4 visible damage process zone (diffuse damage near the crack front) is observed in the present glasses at room
5 temperature (**Figure 3**). Sharp crack tips produced by means of bridge-compression (see **Figure 1** and **2**)
6 were observed by means of optical microscopes, and no blunting could be evidenced for testing temperature
7 below T_g , as shown in **Figure 6a** and **6b** in the case of BPbCuO glasses. Nevertheless, some tip blunting
8 occurs above T_g (**Figure 5** and **6c**). The crack is eventually completely healed at the highest temperature,
9 where the beam deforms in a ductile manner as seen in **Figure 6d**. In such a case, the mechanical work is
10 dissipated in the viscoplastic flow process. **Figure 5b** shows a confined viscoplastic flow region in a
11 BPbCuO glass specimen tested at $1.1 T_g$. The analysis of the growth kinetics of the viscoplastic process zone
12 would be of great interest to understand the physics of cracking and the BDT transition in inorganic glasses.
13 The increase of the plastic zone size with increasing notch tip radius in metallic glasses was discussed in the
14 light of a finite element simulation elsewhere [29], and this is definitely an interesting direction for future
15 investigations on inorganic glasses. Another future investigation, as a key point to understand the crack
16 blunting mechanisms occurring during crack propagation in high temperature, could be the
17 nanocaracterization of crack tips in real time and in high temperature. However, such experiments are
18 extremely hard to be performed.

19 *4.2.Environment dependence of K_{Ic} at room temperature*

20 In the ambient environment (20 °C, RH~60 %), K_{Ic} as measured with a CHS of $0.05 \mu\text{m}\cdot\text{s}^{-1}$ is smaller than
21 that obtained at $5 \mu\text{m}\cdot\text{s}^{-1}$ because at low velocity water molecules in the ambience have the time to react with
22 the oxide bonds at the crack front, mostly Si-O ones, which lowers the energy needed to propagate the crack.
23 This phenomenon is known as stress corrosion [15,18,30]. Taking K_{Ic} values from Table 4 (0.69 and 0.47
24 $\text{MPa}\cdot\sqrt{\text{m}}$ for amorphous Silica measured at a CHS 5 and $0.05 \mu\text{m}\cdot\text{s}^{-1}$ respectively) into Eq. 4, we reach
25 values of 3.38 and $2.15 \text{ J}\cdot\text{m}^{-2}$ for the fracture surface energy. The loss energy is about $1.23 \text{ J}\cdot\text{m}^{-2}$, which
26 corresponds to a 60 % loss of the interatomic bonding energy in average along the crack path. In other word,
27 by taking a new x_i of $1 - 0.6 (= 0.4)$ and applying into Eq. 6 and then 4, we will obtain a value of γ of 2.15

1 $\text{J}\cdot\text{m}^{-2}$ and K_{Ic} of $0.47 \text{ MPa}\cdot\sqrt{\text{m}}$ (the value measured with a CHS of $0.05 \mu\text{m}\cdot\text{s}^{-1}$). Using this loss assumption
2 for SLS, Borofloat and BK7, we obtain K_{Ic} values of 0.53, 0.54 and 0.50, respectively, in good agreement
3 with the experimental results (Table 4).

4 *4.2.1. Indentation crack pattern*

5 The indentation cracking pattern can be studied from the indentation stage of the SEPB method as well as
6 from the post-mortem fracture surface, since the precrack extends through the median plane of the Vickers
7 indents. As discussed above, the precrack length is much greater than the crack created by the indentation,
8 allowing us to avoid humidity influence in the SEPB results, even in the cases where the indentation step is
9 performed in ambient conditions ($20 \text{ }^\circ\text{C}$, RH~60 %) with dwell time of either 15 s or 30 s. However, this
10 difference in indentation dwell time allows us to observe the different indentation cracking pattern in one of
11 the studied glasses, namely BK7. For sake of comparison, the cracking patterns (9.81 N load) of both
12 Borofloat and SLS glasses are shown in **Figure 7**. Cone cracking is observed in the case of Borofloat
13 (**Figure 7a**), quite similar to what is observed in silica glass [31]. This adds more complexity into the
14 analysis of indentation cracking and mostly results in overestimated fracture toughness values as estimated
15 from the radial/median indentation crack length [15]. Semi-elliptical cracks are observed in the case of SLS
16 glass samples (**Figure 7b**). The indentation cracking pattern of the SLS glass was found independent on the
17 dwell time. In contrast, BK7 shows normal radial/median cracks when indented with dwell time of 15 s, but
18 a swollen pattern when indented with dwell time of 30 s. Long dwell time (as in our experiments) may
19 facilitate the reaction of water vapor with the indent, causing some swelling, as seen in **Figure 7b**. It turns
20 out that in the case of swelling, the corner crack length is ~5 to 10 μm shorter.

21 **5. Conclusion**

22 The temperature and environment dependences of K_{Ic} of glasses from different chemical systems were
23 studied by means of the SEPB method. Regarding the effect of temperature, we found that with a loading
24 rate of $4 \text{ MPa}\cdot\sqrt{\text{m}}\cdot\text{s}^{-1}$, a transition from elastic-brittle to viscoplastic-ductile occurs at about $0.9T_g$. Regarding
25 the effect of humidity, the following conclusions were drawn: (i) As long as both the precracking stage and
26 the final fracture in bending are conducted within a one hour period, it is found sufficient to only perform the

1 final fracture stage (in bending) in the dry atmosphere to avoid stress corrosion; (ii) It is sufficient to perform
2 the SEPB experiment in the ambient atmosphere once the cross-head speed (or crack velocity) is fast enough
3 (e.g. a cross-head speed of more than $5 \mu\text{m s}^{-1}$) to prevent against stress corrosion cracking effects on the
4 toughness measurement.

5

6 **Acknowledgements**

7 This work was supported by the European Research Council through the ERC Advanced Grant 320506.

8 **Competing interests**

9 The authors declare no competing financial interests.

10

11 **References**

- 12 [1] J.B. Quinn, I.K. Lloyd, Comparison of Methods to Determine the Fracture Toughness of Three Glass-
13 Ceramics at Elevated Temperatures, *J. Am. Ceram. Soc.* 83 (2000) 3070–3076.
- 14 [2] A. Ghosh, M.G. Jenkins, K.W. White, A.S. Kobayashi, R.C. Brad, Elevated-temperature fracture
15 resistance of a sintered α -silicon carbide, *J. Am. Ceram. Soc.* 72 (1989) 242–247.
- 16 [3] M. Mizuno, H. Okuda, VAMAS round robin on fracture toughness of silicon nitride, *J. Am. Ceram.*
17 *Soc.* 78 (1995) 1793–1801.
- 18 [4] T. Fett, D. Munz, Determination of fracture toughness at high temperatures after subcritical crack
19 extension, *J. Am. Ceram. Soc.* 75 (1992) 3133–3136.
- 20 [5] K.D. McHenry, R.E. Tressler, Fracture Toughness and High-Temperature Slow Crack Growth in SiC,
21 *J. Am. Ceram. Soc.* 63 (1980) 152–156.
- 22 [6] A. Micski, B. Bergman, High temperature strength of silicon nitride HIP-ed with low amounts of
23 yttria or yttria/alumina, *J. Eur. Ceram. Soc.* 6 (1990) 291–301.
- 24 [7] J.J. Brennan, K.M. Prewo, Silicon carbide fibre reinforced glass-ceramic matrix composites

- 1 exhibiting high strength and toughness, *J. Mater. Sci.* 17 (1982) 2371–2383.
- 2 [8] J.L. Henshall, D.J. Rowcliffe, J.W. Edington, Fracture Toughness of Single-Crystal Silicon Carbide,
3 *J. Am. Ceram. Soc.* 60 (1977) 373–375.
- 4 [9] S.M. Wiederhorn, H. Johnson, A.M. Diness, A.H. Heuer, Fracture of glass in vacuum, *J. Am. Ceram.*
5 *Soc.* 57 (1974) 336–341.
- 6 [10] N. Shinkai, R.C. Bradt, G.E. Rindone, Fracture toughness of fused SiO₂ and float glass at elevated
7 temperatures, *J. Am. Ceram. Soc.* 64 (1981) 426–430.
- 8 [11] T. Rouxel, J.-C. Sangleboeuf, The brittle to ductile transition in a soda-lime-silica glass, *J. Non.*
9 *Cryst. Solids.* 271 (2000) 224–235.
- 10 [12] T. Rouxel, Fracture surface energy and toughness of inorganic glasses, *Scr. Mater.* 137 (2017) 109–
11 113.
- 12 [13] T. Rouxel, S. Yoshida, The fracture toughness of inorganic glasses, *J. Am. Ceram. Soc.* 100 (2017)
13 4374–4396.
- 14 [14] G.D. Quinn, J.J. Swab, Fracture toughness of glasses as measured by the SCF and SEPB methods, *J.*
15 *Eur. Ceram. Soc.* 37 (2017) 4243–4257.
- 16 [15] T. To, F. Célarié, C. Roux-Langlois, A. Bazin, Y. Gueguen, H. Orain, M. Le Fur, V. Burgaud, T.
17 Rouxel, Fracture toughness, fracture energy and slow crack growth of glass as investigated by the
18 Single-Edge Precracked Beam (SEPB) and Chevron-Notched Beam (CNB) methods, *Acta Mater.* 146
19 (2018) 1–11. doi:10.1016/j.actamat.2017.11.056.
- 20 [16] T. Nose, T. Fujii, Evaluation of Fracture Toughness for Ceramic Materials by a Single Edge
21 Precracked Beam Method, *J. Am. Ceram. Soc.* 71 (1988) 328–333.
- 22 [17] Q. Zheng, Y. Yue, J.C. Mauro, Density of topological constraints as a metric for predicting glass
23 hardness, *Appl. Phys. Lett.* 111 (2017) 011907-1–5.
- 24 [18] S.M. Wiederhorn, Influence of Water Vapor on Crack Propagation in Soda Lime Glass, *J. Am.*
25 *Ceram. Soc.* 50 (1967) 407–414.
- 26 [19] T. Rouxel, Elastic Properties and Short-to Medium-Range Order in Glasses, *J. Am. Ceram. Soc.* 90
27 (2007) 3019–3039.
- 28 [20] R.E. Youngman, J. Kieffer, J.D. Bass, L. Duffrène, Extended structural integrity in network glasses

- 1 and liquids, *J. Non. Cryst. Solids*. 222 (1997) 190–198. doi:10.1016/S0022-3093(97)90113-7.
- 2 [21] P. Gadaud, S. Pautrot, Characterization of the elasticity and anelasticity of bulk glasses by dynamical
3 subresonant and resonant techniques, in: *J. Non. Cryst. Solids*, North-Holland, 2003: pp. 146–152.
4 doi:10.1016/S0022-3093(02)01947-6.
- 5 [22] K. Tanaka, T. Ichitsubo, E. Matsubara, Elasticity and anelasticity of metallic glass near the glass
6 transition temperature, *Mater. Sci. Eng. A*. 442 (2006) 278–282. doi:10.1016/j.msea.2006.05.161.
- 7 [23] Z. Yao, Synthesis, structure, and mechanical properties of lead-and zinc-copper borate glasses,
8 (2016). <https://www.theses.fr/2016REN1S080> (accessed July 7, 2020).
- 9 [24] T. To, S.S. Sørensen, M. Stepniewska, A. Qiao, L.R. Jensen, M. Bauchy, Y. Yue, M.M. Smedskjaer,
10 Fracture toughness of a metal–organic framework glass, *Nat. Commun.* 11 (2020) 2593.
11 doi:10.1038/s41467-020-16382-7.
- 12 [25] K.M. Flores, R.H. Dauskardt, Enhanced toughness due to stable crack tip damage zones in bulk
13 metallic glass, *Scr. Mater.* 41 (1999) 937–943.
- 14 [26] J.J. Lewandowski, W.H. Wang, A.L. Greer, Intrinsic plasticity or brittleness of metallic glasses,
15 *Philos. Mag. Lett.* 85 (2005) 77–87.
- 16 [27] Y. Shi, J. Luo, F. Yuan, L. Huang, Intrinsic ductility of glassy solids, *J. Appl. Phys.* 115 (2014)
17 043528.
- 18 [28] T. Rouxel, Y. Yokoyama, Elastic properties and atomic bonding character in metallic glasses, *J.*
19 *Appl. Phys.* 118 (2015) 44901.
- 20 [29] P. Tandaiya, R. Narasimhan, U. Ramamurty, Mode I crack tip fields in amorphous materials with
21 application to metallic glasses, *Acta Mater.* 55 (2007) 6541–6552.
- 22 [30] S.M. Wiederhorn, L.H. Bolz, Stress corrosion and static fatigue of glass, *J. Am. Ceram. Soc.* 53
23 (1970) 543–548.
- 24 [31] M.D. Michel, F.C. Serbena, C.M. Lepienski, Effect of temperature on hardness and indentation
25 cracking of fused silica, *J. Non. Cryst. Solids*. 352 (2006) 3550–3555.
- 26 [32] S. Deriano, T. Rouxel, M. Lefloch, B. Beuneu, Structure and mechanical properties of alkali-alkaline
27 earth-silicate glasses, *Phys. Chem. Glas.* 45 (2004) 37–44. [https://hal.archives-ouvertes.fr/hal-](https://hal.archives-ouvertes.fr/hal-01148113)
28 01148113 (accessed July 7, 2020).

- 1 [33] S. Dériano, A. Jarry, T. Rouxel, J.-C. Sangleboeuf, S. Hampshire, The indentation fracture toughness
2 (KC) and its parameters: the case of silica-rich glasses, *J. Non. Cryst. Solids.* 344 (2004) 44–50.
- 3 [34] T. To, C. Stabler, E. Ionescu, R. Riedel, F. Célarié, T. Rouxel, Elastic properties and fracture
4 toughness of SiOC-based glass-ceramic nanocomposites, *J. Am. Ceram. Soc.* 103 (2020) 491–499.
5 doi:<https://doi.org/10.1111/jace.16686>.
6

1 **Tables**

2 **Table 1:** Compositions, mechanical properties and transition temperatures. Results were obtained with a
3 better than 0.005 g·cm³, 2 GPa, 0.01, 2 GPa and 5 K accuracy (experimental error) for ρ , E , ν , G and T_g ,
4 respectively. ¹Data of properties of SiNaMgO and N-Glass are taken from Refs [32] and [33]. ²Planilux
5 (soda-lime silicate, SLS), Saint-Gobain Company.

Glass	compositions	ρ (g.cm⁻³)	E (GPa)	ν	G (GPa)	T_g (K)
SiNaMgO ¹	SiO ₂ (80)Na ₂ O(14)MgO(6)	2.396	66	0.17	28	773
SLS ²	SiO ₂ (71)Na ₂ O(13)MgO(6)CaO(10)	2.495	72	0.23	29	813
N-Glass ¹	SiO ₂ (56)Al ₂ O ₃ (14)Y ₂ O ₃ (24)Si ₃ N ₄ (6)	3.759	137	0.29	53	1207
BPbCuO	B ₂ O ₃ (50)PbO(49)CuO(1)	5.628	64	0.29	25	673

6

1 **Table 2:** Compositions and mechanical properties. Results were obtained with a better than 0.005 g·cm³, 2
 2 GPa, 0.01 and 2 GPa accuracy (experimental error) for ρ , E , ν and G , respectively. ¹Planilux (soda-lime
 3 silicate, SLS), Saint-Gobain Company; ²Silica (amorphous silica, a-SiO₂), Corning Company; ³Borofloat,
 4 Schott Company; ⁴BK7, Schott Company.

Glass	Composition	ρ (g cm⁻³)	E (GPa)	ν	G (GPa)
SLS ¹	SiO ₂ (71)Na ₂ O(13)MgO(6)CaO(10)	2.495	72	0.23	46
a-SiO ₂ ²	SiO ₂ (100)	2.200	70	0.15	30
Borofloat ³	SiO ₂ (81)Na ₂ O(4)B ₂ O ₃ (13)Al ₂ O ₃ (2)	2.211	64	0.20	27
BK7 ⁴	SiO ₂ (70)Na ₂ O(9)B ₂ O ₃ (11)BaO(2)K ₂ O(8)	2.511	82	0.21	34

5

- 1 **Table 3:** Fracture toughness at different temperatures relative to T_g for two loading rates. K_{Ic} is in $\text{MPa}\cdot\sqrt{\text{m}}$
- 2 and the accuracy is better than $0.06 \text{ MPa}\cdot\sqrt{\text{m}}$.

T/T_g	0.35	0.8	0.93	1	1.03	1.05	1.07	1.11
$dK_I/dt = 10 \text{ MPa}\cdot\sqrt{\text{m}}\cdot\text{s}^{-1}$								
$K_{Ic}(\text{SLS})$	0.73	/	0.66	0.64	0.63	0.63	/	Not broken
$K_{Ic}(\text{SiNaMgO})$	0.70	/	/	0.68	/	/	0.62	0.73
$dK_I/dt = 4 \text{ MPa}\cdot\sqrt{\text{m}}\cdot\text{s}^{-1}$								
$K_{Ic}(\text{SLS})$	0.73	/	0.67	0.79	/	/	/	Not broken
$K_{Ic}(\text{SiNaMgO})$	0.70	/	0.61	0.90	/	/	/	Not broken
$K_{Ic}(\text{N-Glass})$	1.04	0.86	1.05	1.08	/	/	Not broken	/
$K_{Ic}(\text{BPbCuO})$	0.43	0.36	0.37	0.44	/	/	Not broken	Not broken

3

1 **Table 4:** Fracture toughness of a window glass (SLS) in argon and ambient atmospheres for two different
 2 displacement rates (cross-head speed). The error interval is the standard deviation calculated from at three
 3 experiments. ⁽¹⁾ Only one experimental result was found valid (due to premature failure).

CHS	Ambient atmosphere (20 °C, RH~60%)		Argon atmosphere (20 °C, RH~0%)	
	5 $\mu\text{m}\cdot\text{s}^{-1}$	0.05 $\mu\text{m}\cdot\text{s}^{-1}$	5 $\mu\text{m}\cdot\text{s}^{-1}$	0.05 $\mu\text{m}\cdot\text{s}^{-1}$
SLS	0.70 ± 0.01	0.55 ± 0.02	0.70 ± 0.02	0.71 ± 0.03
a-SiO ₂	0.69 ± 0.02	0.47 ± 0.05	0.69 ± 0.04	0.71 ± 0.04
Borofloat	0.65 ± 0.03	0.52 ± 0.03	0.67 ± 0.02	0.66 ± 0.05
BK7	0.82 ± 0.02	0.47 ⁽¹⁾	0.81 ± 0.03	0.83 ± 0.04

4

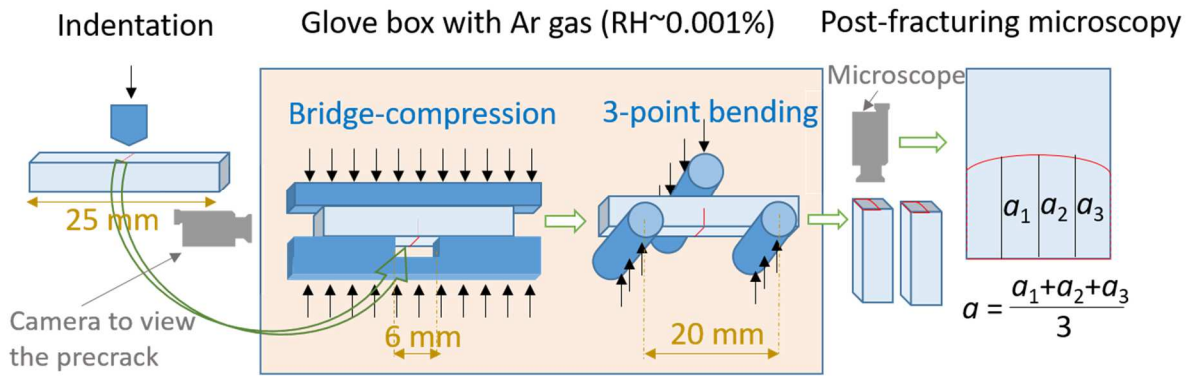
1 **Table 5:** Intrinsic fracture toughness, K_{Ic} , of the four studied commercial glasses: experimental values
 2 (SEPB) and theoretical prediction. \pm : standard deviation calculated from at least three experiments.

Materials	K_{Ic} (MPa\sqrt{m}) by means of SEPB method and Theoretical values			
	Dry Argon atmosphere	Ambient atmosphere (unstable experiment)	Dry N ₂ atmosphere [14] (4-point bending)	Theoretical Prediction [12]
SLS	0.71 \pm 0.03	0.70 \pm 0.01	0.76 \pm 0.03	0.73 \pm 0.01
a-SiO ₂	0.69 \pm 0.04	0.69 \pm 0.02	0.78 \pm 0.06	0.72 \pm 0.01
Borofloat	0.67 \pm 0.02	0.65 \pm 0.03	0.71 \pm 0.03	0.72 \pm 0.02
BK7	0.81 \pm 0.03	0.82 \pm 0.02	0.92 \pm 0.05	0.85 \pm 0.01

3

4

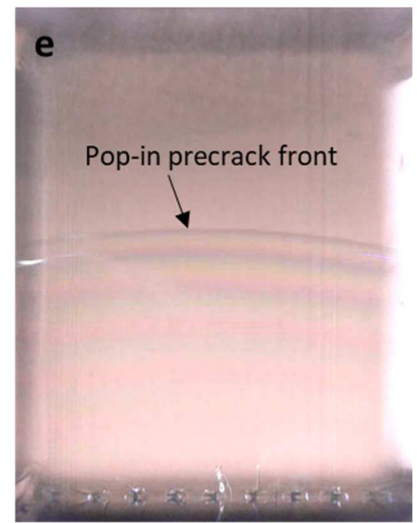
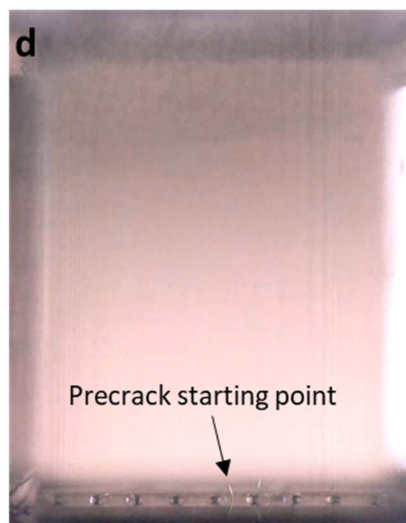
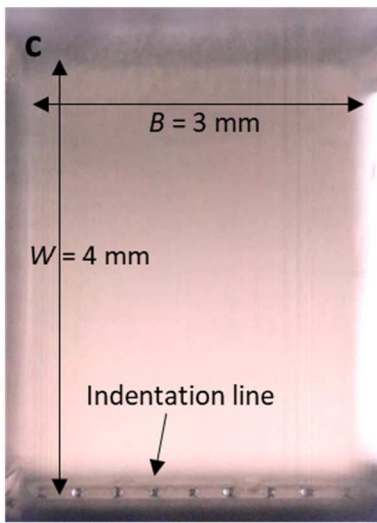
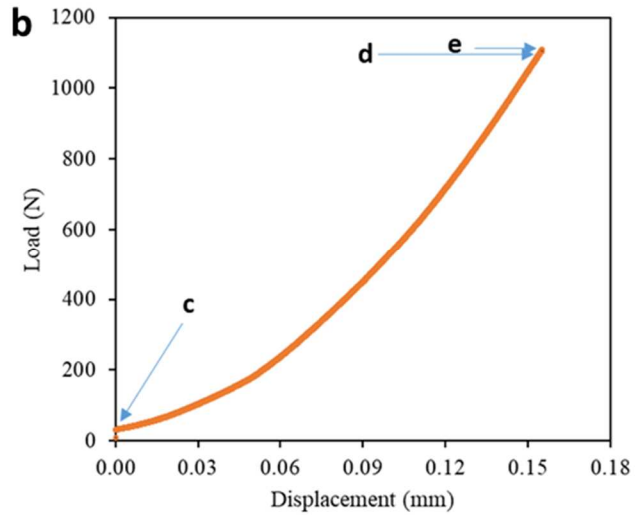
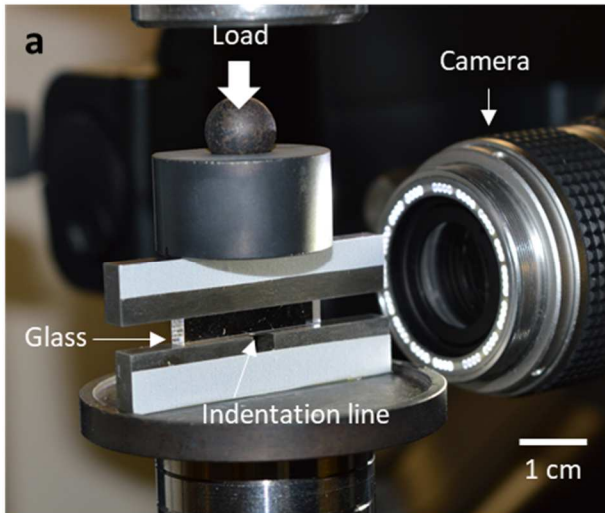
1 **Figures**



2

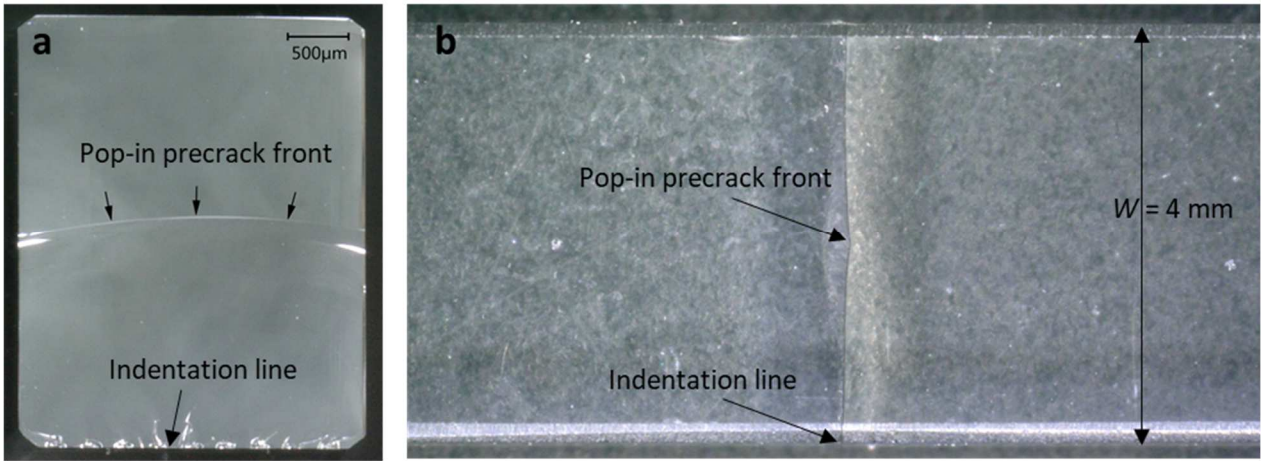
3 **Figure 1:** Schematic drawing of the SEPB experiment from indentation to precrack (a) measurement. Both
 4 precracking (by bridge compression) and fracturing (by 3-point bending) were performed in the glove both to
 5 assure the non-humidity environment. It is noteworthy that although the indentation was performed outside
 6 the glove box, there would not be any humidity left after the precracking stage since a is ~100 times longer
 7 that the indentation depth. The black narrow, dark blue block and light blue block represents the applied load
 8 (or stress), the equipment and glass specimen, respectively. The red lines represents the indentation line and
 9 precrack front.

10



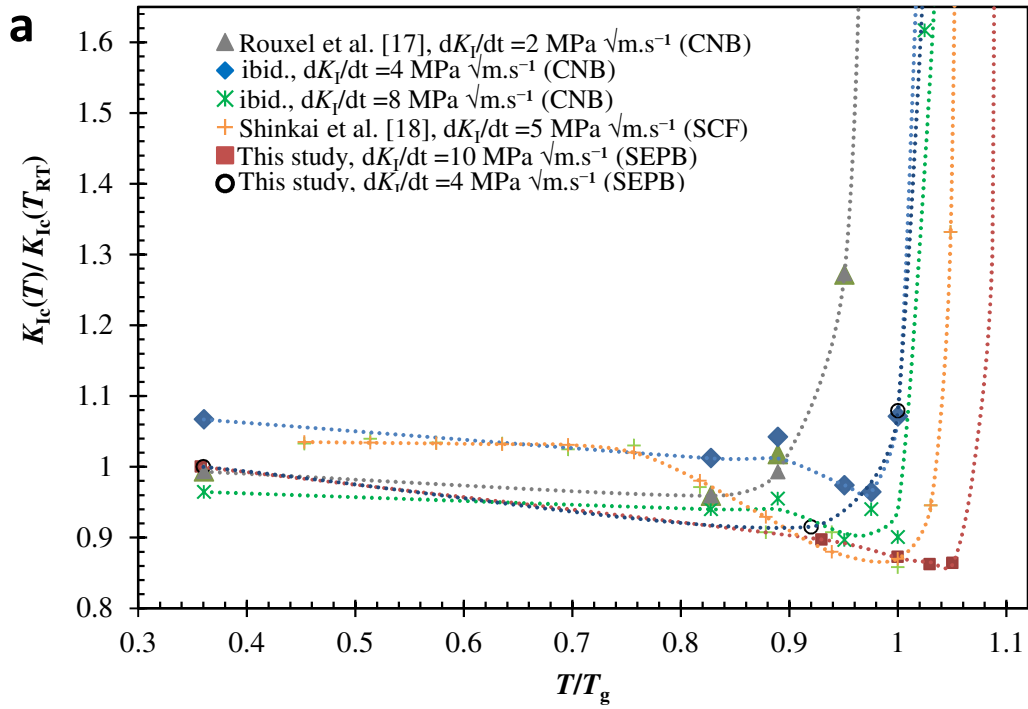
1

2 **Figure 2:** Precracking observation on a soda-lime-silica glass SEPB specimen. **a.** Bridge-compression
 3 fixture with an optical camera. **b.** The load-displacement curve from the bridge-compression test. The point
 4 c, d and e are according to **c.** The initial state of the SEPB specimen focused on the middle part, where the
 5 indentation line is located, with visible indentation line at the bottom. **d.** the precrack starting point from
 6 joint crack of two indents around the middle of the indentation line as shown by the black arrow. **e.** the
 7 precrack front; the precrack is visible in rainbow colors. The light orange color in the 2c, 2d and 2e is from
 8 the lamp installed in the room (the brightness at the right-hand side of 2c, 2d and 2e). The precracking
 9 observation on a non-transparent glass is made possible by positioning the camera on the sample side
 10 (perpendicular to the current position) as shown elsewhere [34].

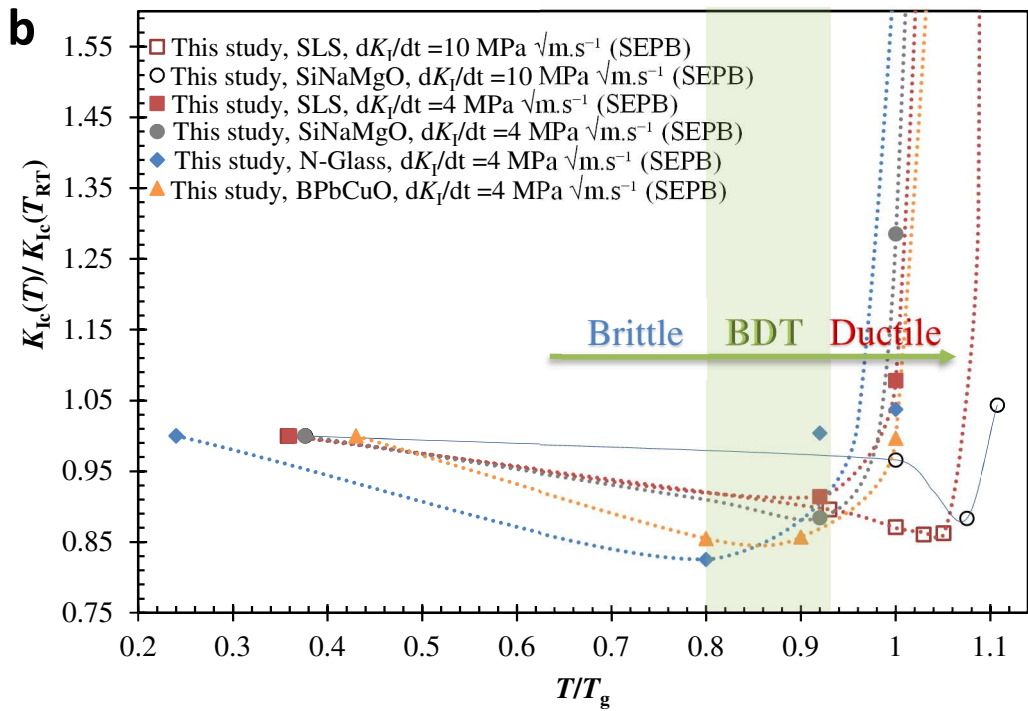


1

2 **Figure 3:** Post-fractography on the same glass specimen used in **Figure 2**. **a.** Typical image used for
3 measuring the precrack length at 25%, 50% and 75% of the broadness, B (**Figure 2**). In this case, the
4 precrack evenness (the difference between the average length and any measured length) is around 0.2%, i.e.
5 valid precrack [15]. **b.** Typical side view of two broken pieces positioned close to each other and used to
6 measure the angle of the fracture plan (the plan after precrack front). In this case, the angle is around 1° , i.e.
7 valid test.



1

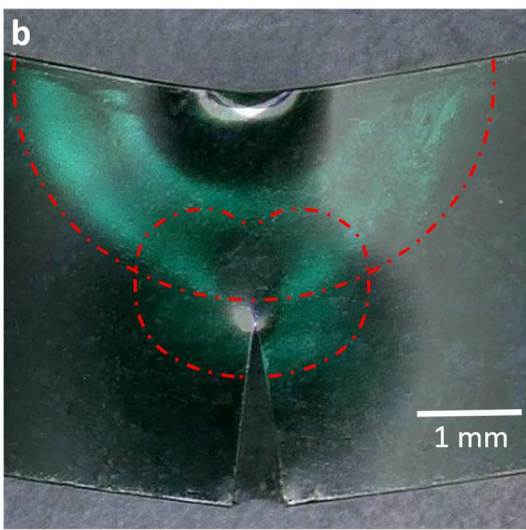


2

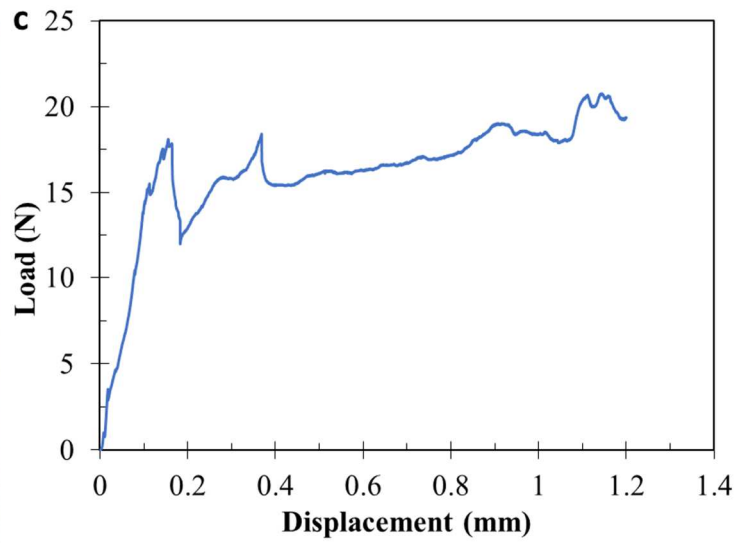
3 **Figure 4:** Temperature dependence of the apparent fracture toughness of **a.** soda-lime silicate (SLS) with
 4 different loading rates and **b.** all studied glasses with a loading rate of $4 \text{ MPa}\cdot\sqrt{\text{m}}\cdot\text{s}^{-1}$, and additional SLS and
 5 SiNaMgO with a loading rate of $10 \text{ MPa}\cdot\sqrt{\text{m}}\cdot\text{s}^{-1}$. Rouxel et al. [11] used chevron-notched beam (CNB)
 6 method and Shinkai et al. [10] used surface crack in flexure (SCF) method. The horizontal green narrow
 7 shows the brittle to ductile states of the four studied glasses when using the rate of $4 \text{ MPa}\cdot\sqrt{\text{m}}\cdot\text{s}^{-1}$.



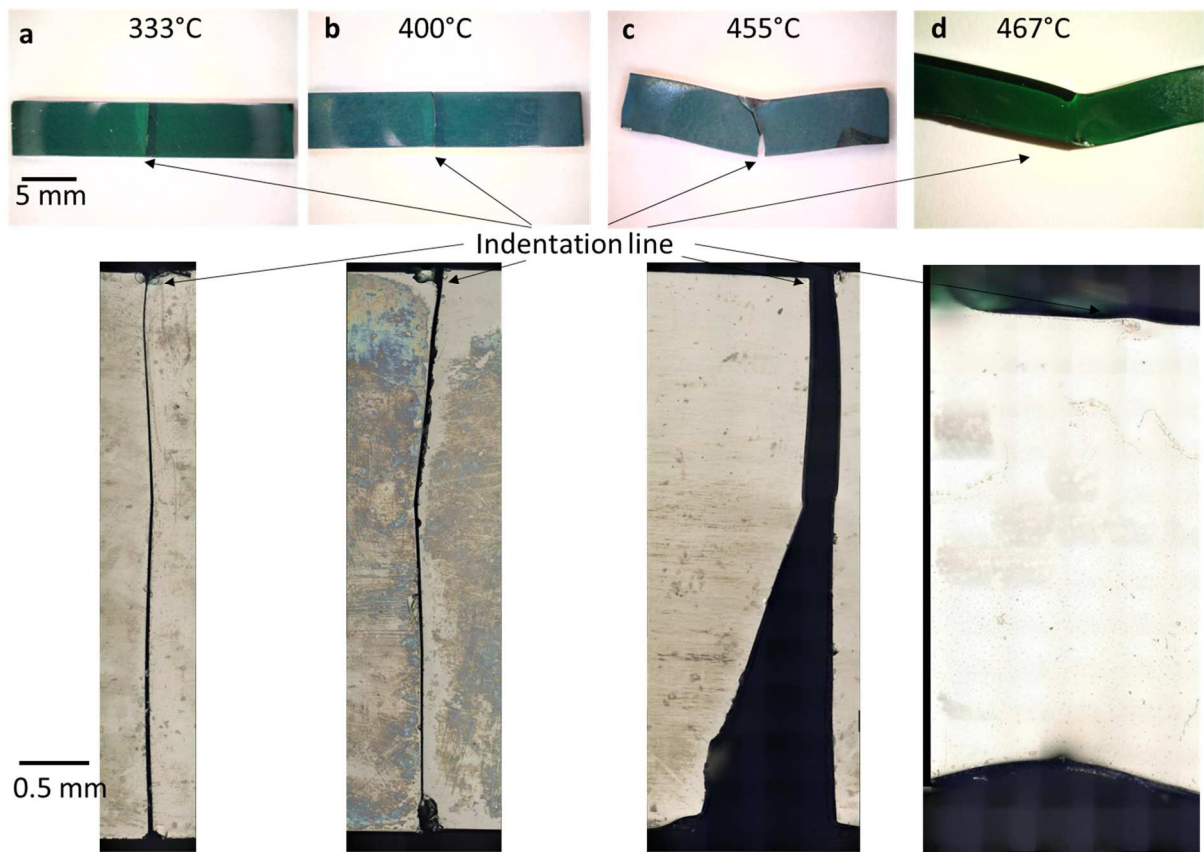
1



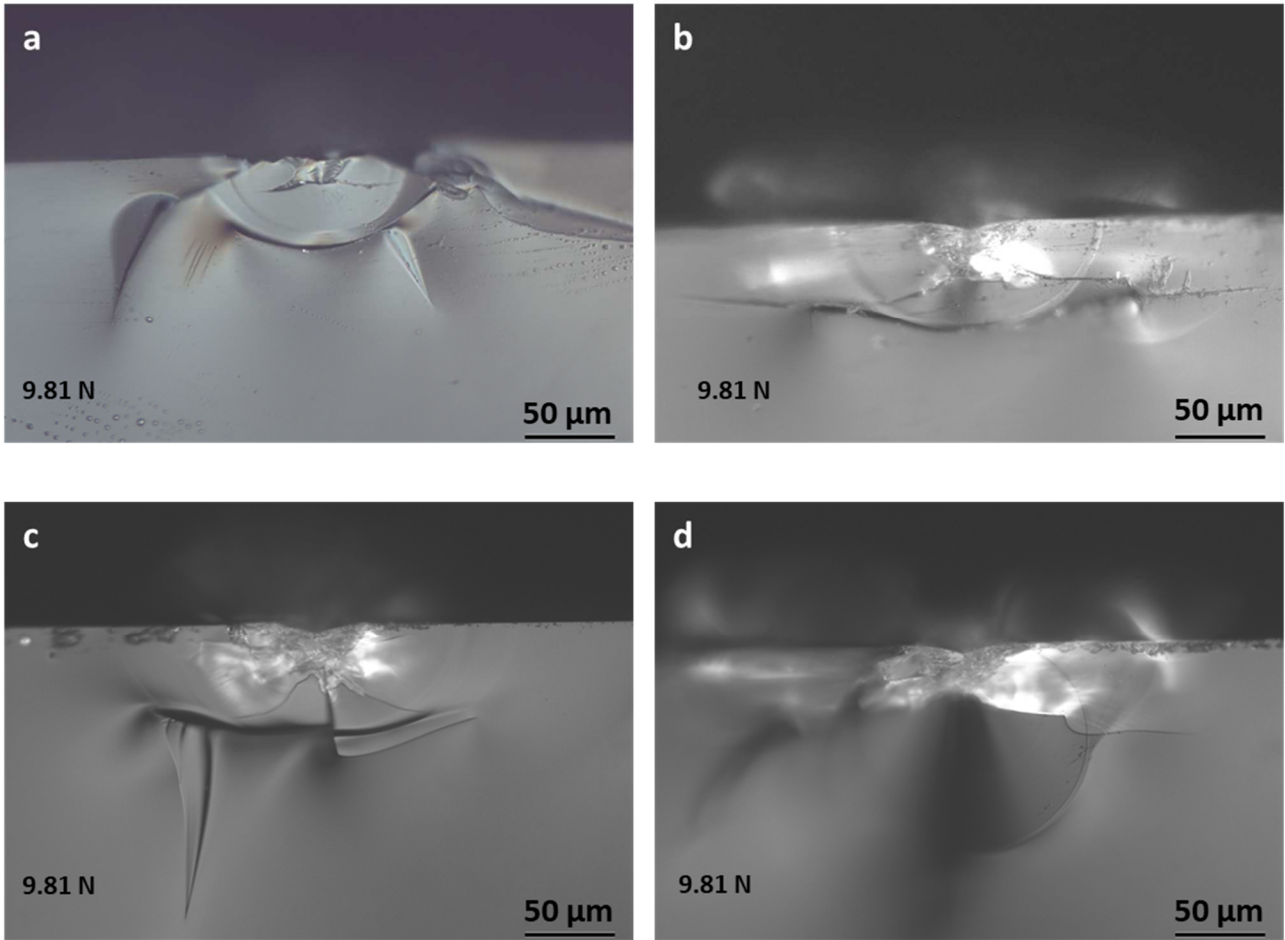
2



3 **Figure 5:** A BPbCuO glass specimen tested in bending at $\sim 1.1T_g$ with a loading rate of $4 \text{ MPa}\cdot\sqrt{\text{m}\cdot\text{s}^{-1}}$,
4 exhibiting viscoplastic deformation without fracture: **a.** after cooling down to room temperature; **b.** zoom
5 around the crack tip (the red dashed line contour shows the shape of the confined viscoplastic zone around
6 the crack front and just beneath the upper roller); **c.** corresponding load-displacement curve.



1 ,
 2 **Figure 6:** Pre-crack tip analysis on BPbCuO glasses tested in temperatures from 333°C to 467°C. Upper: 2
 3 broken pieces of SEPB specimen with the indentation line at the bottom (black arrow). Lower: Zoom on the
 4 fracture plane. The degradation on the surfaces were from the heating, cooling and storage processes.



1

2 **Figure 7:** Indentation pattern (cross section) observed from the indentation line in the post-fractured
3 precrack image as shown in **Figure 3a**. **a.** Borofloat glass, **b.** SLS, **c.** and **d.** BK7. The different between **c**
4 and **d** is the indentation dwell time. **c** use the dwell time of 15s and **d** of 30s.